Journal of Structural Geology 33 (2011) 676–689

Contents lists available at ScienceDirect

Journal of Structural Geology

journal homepage: www.elsevier.com/locate/jsg

Crack-seal microstructure evolution in bi-mineralic quartz–chlorite veins in shales and siltstones from the RWTH-1 well, Aachen, Germany

Stephan Becker [a,*], Christoph Hilgers [b], Peter A. Kukla [a], Janos L. Urai [c]

[a] Geological Institute, RWTH Aachen University, Wüllnerstraße 2, D-52056 Aachen, Germany
[b] Reservoir Petrology, RWTH Aachen University, Wüllnerstraße 2, D-52056 Aachen, Germany
[c] Structural Geology, Tectonics and Geomechanics, RWTH Aachen University, Lochnerstraße 4-20, D-52056 Aachen, Germany

ARTICLE INFO

Article history:
Received 25 February 2010
Received in revised form
23 December 2010
Accepted 6 January 2011
Available online 20 January 2011

Keywords:
Microstructures in syntectonic veins
Crack-seal
Polycrystal growth in bi-mineralic veins
2D simulations of crystal growth

ABSTRACT

In core samples from the deep geothermal well RWTH-1 we studied Variscan quartz–chlorite veins formed by crack-seal processes in siliciclastics at the brittle to ductile transition. These sheared veins are common in sections of the well, which are interpreted as Variscan thrust zones based on image logs and seismic data. Microstructures interpreted to reflect different stages in the evolution of such crack-seal veins suggest the veins started in microcracks sealed by quartz and chlorite, to veinlets crossing multiple grains, and bundles of veinlets evolving by progressive localization into low-angle extensional shear veins and high-angle dilational jog veins. In the sheared veins, chlorite and quartz ribbons show evidence for crack-seal and simultaneous ductile shearing during vein evolution, forming peculiar fin-shaped microstructures in quartz ribbons. In high-angle dilational jogs fibrous crystals of quartz and chlorite point to multiple crack-seal events with simultaneous growth of two different mineral phases. This is interpreted to be the basic microstructural process in the veins. We extend earlier models of polycrystal growth in fractures and present a series of 2D simulations of the kinematics of crystal growth in these bi-mineralic veins for both localized and non-localized cracking. Results are compared with the observed microstructures. We show that when the relative growth rates of the two mineral phases are different, serrated grain boundaries evolve. The similarities between observation and model suggest that the assumption of our model is valid, although many second order processes require a more detailed study. We propose that the principles observed here can be applied to other bi-mineralic crack-seal veins.

1. Introduction

Syntectonic crack-seal veins form by repeated fracturing and healing and show a wide range of microstructures from blocky to fibrous (Durney and Ramsay, 1973; Ramsay, 1980). Microstructures such as crystal shape, the arrangement of inclusions and sometimes even fiber boundaries in veins can be a unique tool to deduce the opening kinematics of fractures and the deformation history of rocks (Taber, 1916; Grigor'ev, 1965; Ramsay and Huber, 1983; Urai et al., 1991; Hilgers et al., 2001). Although many veins in nature contain two or more mineral phases most studies focus on mono-mineralic crack-seal veins. Here, we examine bi-mineralic quartz–chlorite veins formed in dilational jogs. We analyze the range of microstructures and the geometry of fibrous grain boundaries.

Crystals growing in dilational jogs may form blocky aggregates, if growth is anisotropic and in free fluid (Fisher and Brantley, 1992; Bons and Jessell, 1997; Nollet et al., 2005). However, they may become elongate-blocky or fibrous microstructures during fracture sealing, if in repeated contact with the wall rock. These elongate-blocky to fibrous microstructures are called ataxial, syntaxial and antitaxial (Durney and Ramsay, 1973; Passchier and Trouw, 1996).

Antitaxial microstructures ("truly fibrous" after Bons, 2000) form by cracking at the vein wall with fiber growth from the vein center towards the wall rock (Grigor'ev, 1965; Durney and Ramsay, 1973; Cox and Etheridge, 1983; Urai et al., 1991; Hilgers et al., 2001). Numerical simulations show a continuous transition from elongate-blocky to fibrous vein microstructures growing towards a wall, with the crack aperture, crystal growth rate, the wall rock roughness and the number of increments governing the final microstructures and the tracking capability of fiber grain boundaries (Urai et al., 1991; Bons, 2001; Hilgers et al., 2001; Nollet et al., 2005).

In contrast, *syntaxial* vein microstructures grow from the wall rock towards the center of the vein, which is often indicated by a median line. Growth competition of neighboring crystals results in an elongate-blocky microstructure. Growth takes place in the center of the vein (Ramsay and Huber, 1983). In some cases, the

* Corresponding author. Fax: +49 (0)241 8092151.
E-mail address: becker@geol.rwth-aachen.de (S. Becker).

0191-8141/$ – see front matter © 2011 Elsevier Ltd. All rights reserved.
doi:10.1016/j.jsg.2011.01.001

arrangement of inclusions can be used to deduce the opening trajectory of the vein (Cox and Etheridge, 1983).

Ataxial veins (called stretched crystals in Durney and Ramsay, 1973) also display a elongate-blocky microstructure but cannot be used to deduce the opening history of the vein (Cox and Etheridge, 1983; Hilgers and Urai, 2002; Bons and Jessell, 1997). They can clearly be distinguished from antitaxial microstructures by their sawtooth-shaped grain boundaries and vein minerals *not* being detached from the grains in the wall rock. Furthermore, many ataxial veins clearly show multiple inclusion bands aligned parallel to the vein wall, indicating multiple crack-seal increments and non-localized cracking (e.g. Ramsay, 1980; Dietrich and Grant, 1985; Lee and Wiltschko, 2000; Laubach et al., 2004b). Cervantes and Wiltschko (2010) recognized a transition from a group of single filled fractures at the vein tip (also called veinlets) to wall-normal fibers at the central region of the vein which developed as a result of repeated fracturing and filling of host rock grains (at the vein walls) or fibers.

Inclusions are frequently observed in dilational jog veins, which can be used to infer the opening history of the vein. These can be fluid inclusions in bands oriented parallel to the crack-seal microfractures, host rock inclusions (lithons) displaced from the wall rock, and other minerals precipitated during vein growth (e.g. Koehn and Passchier, 2000). Host rock lithons being sliced off during shearing are incorporated into the vein during incremental slip and have been shown to detach in sequence into dilational jog veins (e.g. Gaviglio, 1986; Lee and Wiltschko, 2000). The orientation of stress trajectories within dilational jog veins were deduced from numerical modeling and photoelasticity experiments (Ohlmacher and Aydin, 1997; Connolly and Cosgrove, 1999; Fletcher and Pollard, 1999; Soliva et al., 2010).

In this paper, we present an analysis of dilational jog veins with ataxial microstructures. These veins consist of two mineral phases (bi-mineralic) with a number of new, previously not described diagnostic microstructures. We then present a model which explains the formation of serrated grain boundaries by polycrystal growth in poly-mineralic fractures. Further we present a useful method to trace the variation of stress orientation inside the vein. Finally we develop a model of poly-mineralic vein formation evolving from (1) non-localized veinlets in single grains, towards (2) a bundle of veinlets in the host rock into (3) a fully developed crack-seal vein.

2. Geological setting

The RWTH-1 well is located in the city center of Aachen (Germany) at the north-western part of the Rhenish Massif in the Central European Variscan Orogen (Fielitz, 1992; Fielitz and Mansy, 1999; Hollmann and von Winterfeld, 1999; Hance et al., 1999; Oncken et al., 1999; Walter, 2007) (Fig. 1A,B). The Variscan fold-and-thrust belt is characterized by NW-verging folds and mainly SW-dipping thrusts which cause repetition of the Paleozoic sequence (Fig. 1C,D). Variscan deformation and metamorphism took place between 336 and 300 Ma (Nierhoff, 1994) with an overall shortening of around 45% (Hollmann and von Winterfeld, 1999).

The Lower Rhine Embayment rift system started to form during the Mesozoic with periods of extension and inversion (Zijerveld et al., 1992; Worum et al., 2005) and is still active with NW-SE-trending normal faults and active seismicity. The RWTH-1 well is located in the transition zone between the subsiding Lower Rhine embayment and the uplift of the Rhenish Massif (Geluk et al., 1994; Kooi et al., 1998; Garcia-Castellanos et al., 2000; Demoulin and Hallot, 2009), in the intensively deformed footwall of the imbricated front of the Variscan fold-and-thrust belt, about 500 m north of the frontal Variscan thrust with a displacement of 17 km (Hollmann and von Winterfeld, 1999). The closest major Cenozoic normal fault of the Lower Rhine Embayment rift is the poorly defined Laurensberg Fault System 400 m WSW of the well (Fig. 1C).

The RWTH-1 well (MD = 2544 m) was logged using a suite of high resolution instruments and cored in three intervals. Results show a strongly deformed, deeply buried Paleozoic sequence overprinted by both the Variscan compression and Meso- to Cenozoic extension phases, manifested by multiple generations of veins, faults, folds and cleavages and a complex present day stress state (Trautwein-Bruns et al., 2010). The uppermost 20 m penetrated are Pleistocene and Upper Cretaceous clastic sediments (Kukla et al., 2002), that unconformably overly Upper Carboniferous coal-bearing siliciclastic rocks (20–1012 m depth) from the Namurian stages A–C and the Westfalian A (Ribbert, 2006) (Fig. 2A). Immediately below the Upper Carboniferous, the Condroz-beds of the Upper Devonian were encountered at 1012–1260 m, consisting of gray, interbedded siltstones and fine-grained sandstones. The Upper Fammnenian shales, from 1260 m to 1408 m, are gray shaly siltstones with interbedded, fine-grained, quartz- or carbonate-cemented, thin sandstones. The section between 1408 m and 1438 m comprises two nodular carbonate layers (thickness of 2 and 10 m, respectively) separated by a siliciclastic unit. Conodont data indicate the Crepida – zone of the Upper Devonian Nehden-stage (Piecha, 2007). Below 1438 m the well penetrated a sequence of red-green and gray silty shales in the upper part (until 1895 m) and gray, silty sandstones with intercalated thin layers of red and green silty shales between 1895 and 2400 m.

The Devonian and Carboniferous carbonate units and the complete Middle Devonian, which are well known from the surface geology in the hanging wall of the Variscan thrust, were absent in the borehole due to regional facies changes between the rocks from the footwall and rocks from the hanging wall.

The three cored sections (1392–1515 m, 2128–2142 m and 2536–2544 m) (Fig. 2A) of the well contain hydrothermal veins of Variscan and post-Variscan age (Scholz et al., 2006; Sindern et al., 2007, 2008; Lögering, 2008; Chatziliadou, 2009). In the region, Variscan veins have homogenization temperatures up to 400 °C and salinities of around 10 wt.% NaCl equivalent while post-Variscan fluids show homogenization temperatures <250 °C at high salinities of around 20 wt.% NaCl equivalent (e.g. Muchez and Sintubin, 1998).

In agreement with the regional picture, Lögering (2008) distinguished three types of syntectonic Variscan veins in the RWTH-1 core: quartz-carbonate ± chlorite, carbonate ± chlorite and quartz ± chlorite (studied in this paper). Fluid inclusion analyses suggest that the hydrothermal veins were formed at 280–390 °C and low salinities of fluids (<9 wt.%) during lower greenschist facies metamorphism (Lögering, 2008), similar to the Variscan tectonic brines described by others (e.g. Behr et al., 1987; Muchez and Sintubin, 1998).

Temperatures of the Variscan hydrothermal event forming veins are higher than those reported from the host rock in the footwall of the frontal Variscan thrust of approximately 200 °C (Hollmann, 1997; Rottke and Stroink, 1999; Sindern et al., 2007). While illite crystallinity in the host rock in the RWTH-1 well indicates temperatures <200 °C and represents the peak burial of the rock, chlorite was shown to grow syntectonically in veins and cleavage bandsup to anchizonal grade (Sindern et al., 2007). Sindern et al. (2007, 2008) conclude that the high epizonal temperatures derived from fluid inclusions (Lögering, 2008) and vitrinite reflectance (Oncken et al., 1999) in the vicinity of the Aachen thrust can only be correlated with the lower temperatures derived from illite and chlorite crystallinities by the expulsion of tectonic brines during Variscan thrusting and thrust loading over a period of less than 10,000 years. Expulsion of brines along thrusts in the footwall of the Aachen thrust is also indicated by trace element distributions from borehole cuttings (Sindern et al., 2008), which mirrors the

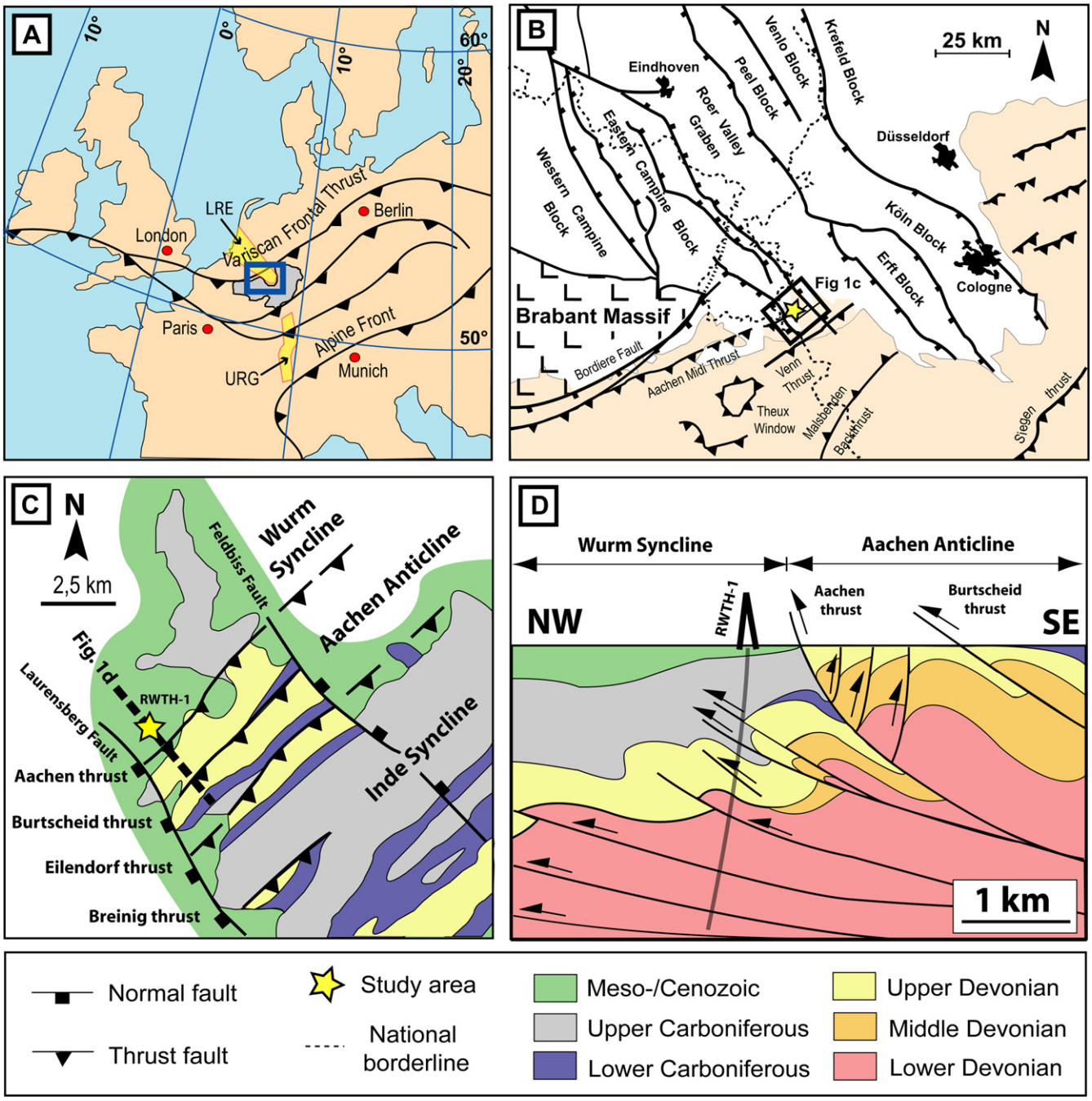

Fig. 1. A) The study area is located at the frontal thrust of the Mid-European Variscides and in the south-western part of the Lower Rhine Embayment rift zone. (LRE – Lower Rhine Embayment, URG – Upper Rhine Graben) B) Geological map of the northern part of the NE-SW striking Variscan fold-and-thrust belt and the Lower Rhine Embayment with its NW-SE striking normal faults. The Variscan Paleozoic rocks (orange) are unconformably overlain by Meso- and Cenozoic sediments (white) (based on Blundell et al., 1992; de Vos et al., 1993; Geluk et al., 1994 and Walter, 2007). C) Detailed geological map of the Variscan fold-and-thrust belt of the Aachen region (modified from Walter, 2010). The RWTH-1 well is located in the city center of Aachen, at the transition zone between the seismically active Lower Rhine embayment with NW-SE striking normal faults and the Variscan fold-and-thrust belt. D) Geological cross section across the northern part of the Variscan fold-and-thrust belt of the Aachen region (modified from Sindern et al., 2008). Note that the RWTH-1 well is located ca. 500 m NW of the frontal Variscan thrust and drilled through the folded and imbricated footwall of the thrust sheet. (For interpretation of the references to color in this figure legend, the reader is referred to the web version of this article).

sediment sources as well as the diagenetic and hydrothermal overprinting (Milliken, 2003).

3. Methods

The details of logging and coring and related data-acquisition in the RWTH-1 well are described elsewhere (Trautwein-Bruns et al., 2010). We studied all cores and took about 100 samples containing quartz–chlorite veins from the cored intervals. They were cut perpendicular to the veins and parallel to slickensides in the plane of the vein where possible. Polished thin sections (4.8 cm × 2.8 cm) with a thickness of 30 μm were used for microstructural studies. For cathodoluminescence studies, we used the hot CL (type: HC-1 LM; Neuser, Bochum, Germany) run at a voltage of 14 kV with a beam current density of 0.6–0.75 mA/mm^2. Core samples were oriented by matching the corescan with FMI-log data.

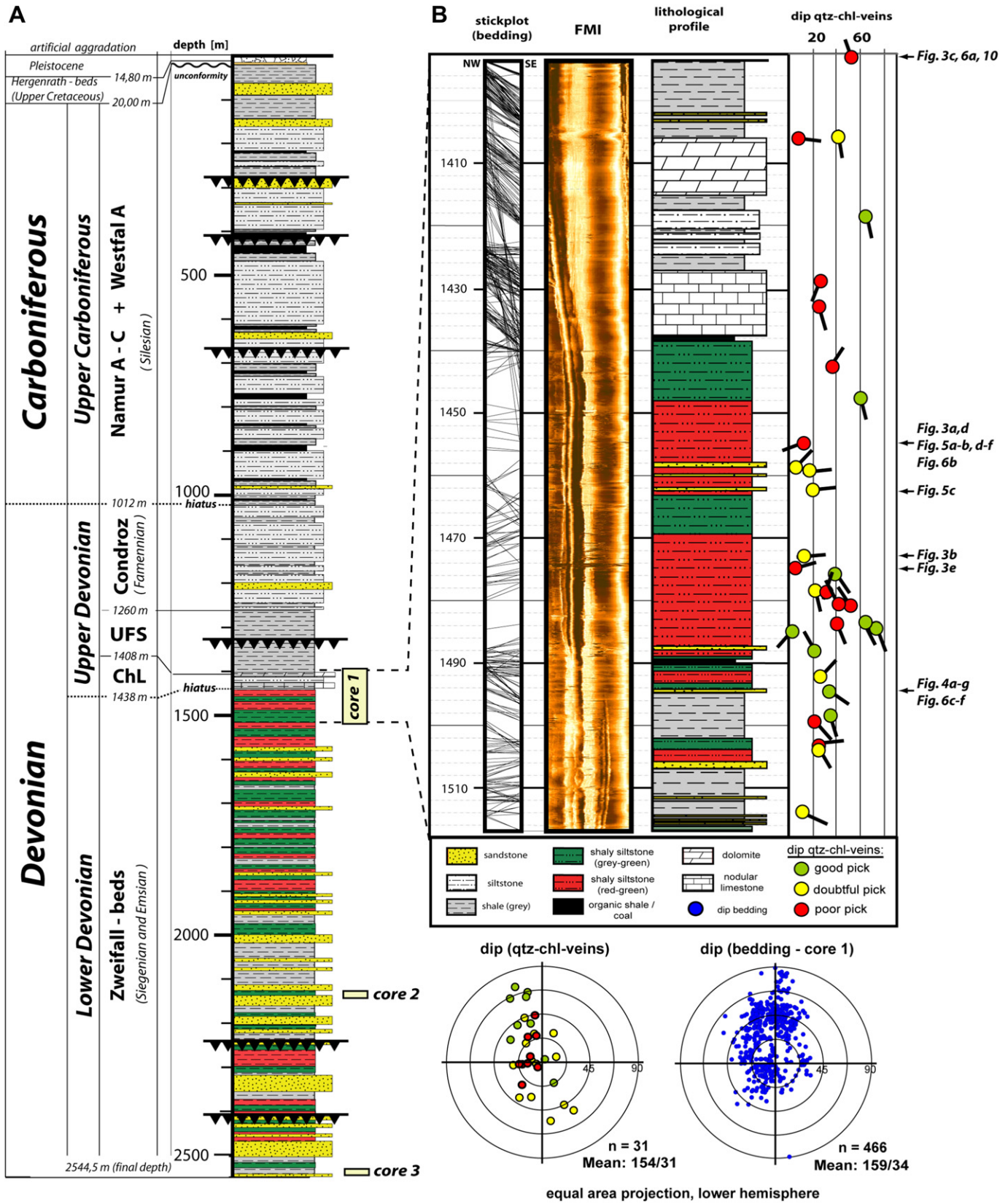

Fig. 2. A) Lithological profile of the RWTH-1 well (modified from Ribbert, 2006). The well penetrated mainly Upper Carboniferous and Devonian strata unconformably overlain by a thin package of Meso- and Cenozoic sediments. Several fault zones were identified in the well based on well logging data and seismic interpretation (Becker, 2008; Trautwein-Bruns et al., 2010). The three cored sections (1392–1515 m, 2128–2142 m and 2536–2544 m) are shown on the right hand side of the figure. B) Detail of the 1st core section, illustrating the lithology and dip of bedding (stick plot and stereonet) vs. fractures and break-outs (FMI-log). Variscan quartz–chlorite veins are restricted only to the 1st core section and are absent in the other cored sections. The location and dip of quartz–chlorite veins in the 1st core section is highlighted in the tadpole plot on the right side and in the stereonet, showing an overall dip towards SE directions. (UFS – Upper Fammenian shales, ChL – Cheiloceras limestone).

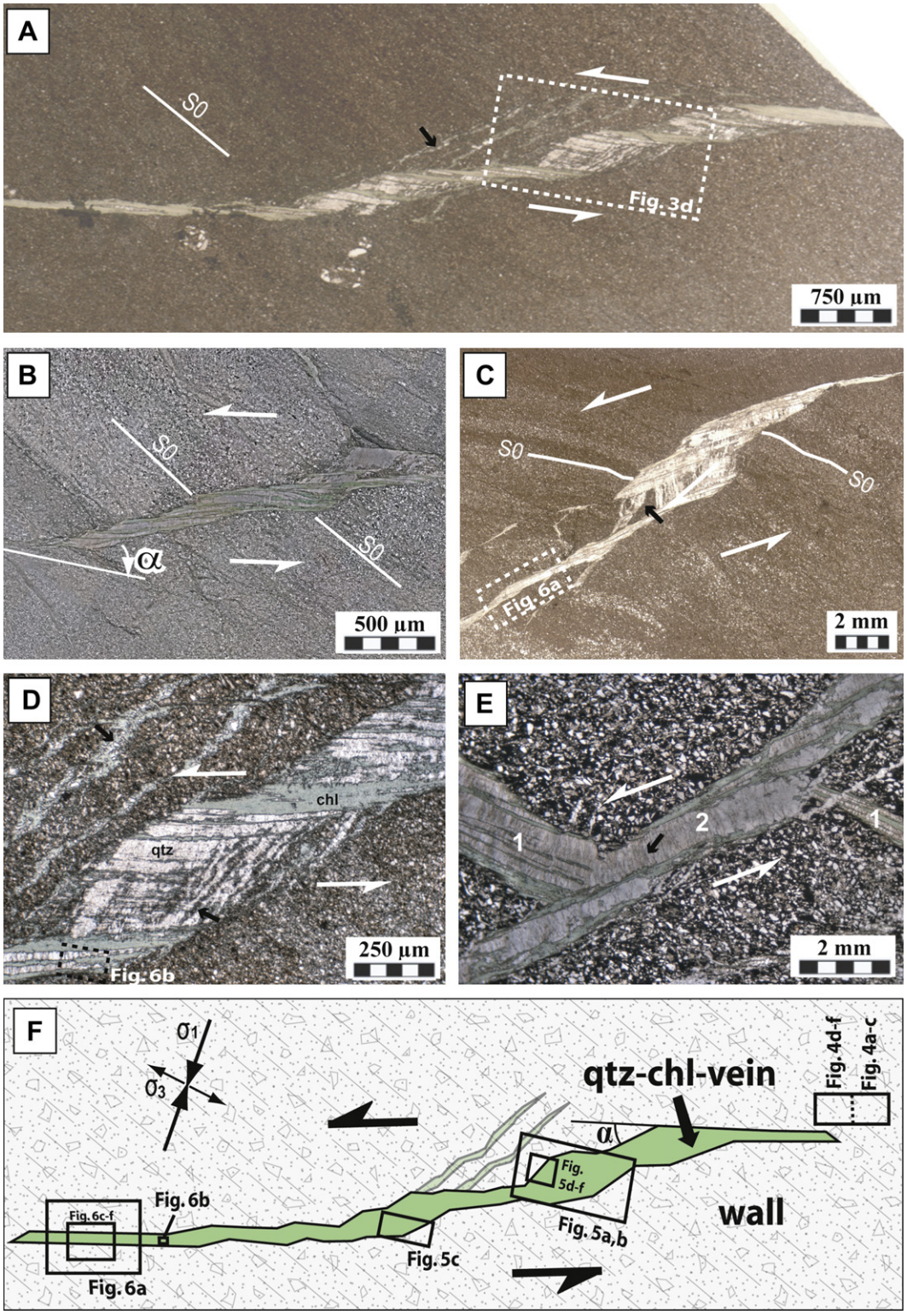

Fig. 3. A) Overview of a typical quartz–chlorite vein consisting of three thick high-angle dilational jog veins in the center of the image and thin extensional shear veins on both ends of the vein. Notice the incipient veins oriented parallel to the thick high-angle jog (black arrow). Box outlines the area covered by Fig. 3D. B) Thin extensional shear vein (low α-angle of around 15°) and a thick high-angle dilational jog vein in the upper right corner of the image. Note that the overall orientation of chlorite and quartz fibers is constant across the vein, indicating a simultaneous formation of low-angle extensional shear vein and high-angle dilational jog vein as one. C) Overview of a high-angle dilational jog vein (high α-angle $> 50°$). The occurrence of lithons (black arrow) and chlorite inclusion trails indicates that the vein formed by multiple crack-seal increments. Lithons indicate non-localized cracking in the host rock, while chlorite inclusion bands and trails show a more localized cracking in the vein. Notice the offset of the bedding (S0). Box outlines the area covered by Fig. 6A. D) Detail of the high-angle dilation jog vein shown in Fig. 3A with lithons arranged as inclusion bands (lower black arrow) and quartz (qtz) and chlorite (chl) fibers crossing the vein. Notice the low-angle extensional shear vein at the lower left corner of the image and the occurrence of several incipient veins (upper black arrow) in the surrounding host rock. Both quartz and chlorite fibers in the low-angle extensional shear vein are oriented parallel to the same fibers in the high-angle dilational jog vein. Similarly, the crack-seal inclusion bands within the white quartz minerals are parallel to the ones in the high-angle dilational jog vein, indicating synchronous formation of both vein structures. Box outlines the area covered by Fig. 6B. E) Two generations of quartz–chlorite veins with clear overprinting relationships. The older vein (1) is truncated by a younger vein (2) and was also sheared. Both veins show the same mineralogical and microstructural inventory, suggesting that the two veins formed in the overall same tectonic setting. F) Schematic illustration of a quartz–chlorite dilational jog vein outlining the positions of the microstructures shown on the following figures.

4. Results

The distribution of quartz–chlorite veins is heterogeneous along the 1st core section of the RWTH-1 well (Fig. 2B). Vein density is lowest in the uppermost section: Only 6 veins were observed in the Upper Devonian section between 1392 and 1438 m, while the section between 1438 and 1515 m (Lower Devonian) contains 23 veins. No veins were observed in the other two cores at 2128 m and 2536 m depth.

The quartz–chlorite veins of this study usually dip at about 30° to SE and have an angle to bedding of around 30° (Fig. 2B). The veins commonly show an offset of markers which can be thin layers of bedding, cleavage domains or other veins (Fig. 3A–C).

We interpret the increased occurrence of shear veins in the interval between 1438 and 1515 m to be related to a Variscan thrust zone, indicated by their orientation, homogenization temperatures and salinities (Lögering, 2008), and the presence of cataclasites at a depth of 1512.95 m together with the distribution of trace elements (Sindern et al., 2008).

4.1. Age relationships (quartz–chlorite veins)

We found several generations of quartz–chlorite veins, indicated by clear overprinting relationships. In intersecting veins the microstructures and mineralogy are very similar, indicating similar conditions of formation (cf. Fig. 3E).

4.2. Microstructural inventory

The quartz–chlorite veins contain a wide range of microstructures (Fig. 3). At the cm-scale the vein morphology can be characterized by the branching angle α, which Soliva et al. (2010) defined as the angle between the slipped structure and the branching jog (Fig. 3B,F). The veins show a variety of branching angles with two end-member microstructures of quartz–chlorite veins: high-angle veins emplaced in dilational jogs with $\alpha > 50°$ and low-angle extensional shear veins with $\alpha < 10°$. An example of such transition is shown in Fig. 3C, where a low-angle extensional shear vein in the lower left corner grades into a high-angle vein in the middle part of the picture and in the upper right corner it becomes again a low-angle extensional shear vein. Similar features can be observed in Fig. 3D, where the high-angle dilational jog vein tapers off into a low-angle extensional shear vein (lower left corner). Below, we discuss the microstructures of the different types of veins.

4.2.1. Veinlets

The host rock locally contains thin, transgranular, healed microfractures (thickness: 5–20 μm) (Fig. 4). In a number of cases these are associated with the tips of shear veins. One important observation is that the quartz grains in the healed microfractures are often longer than the diameter of the broken quartz grains (Fig. 4), creating the characteristic sawtooth-microstructure of

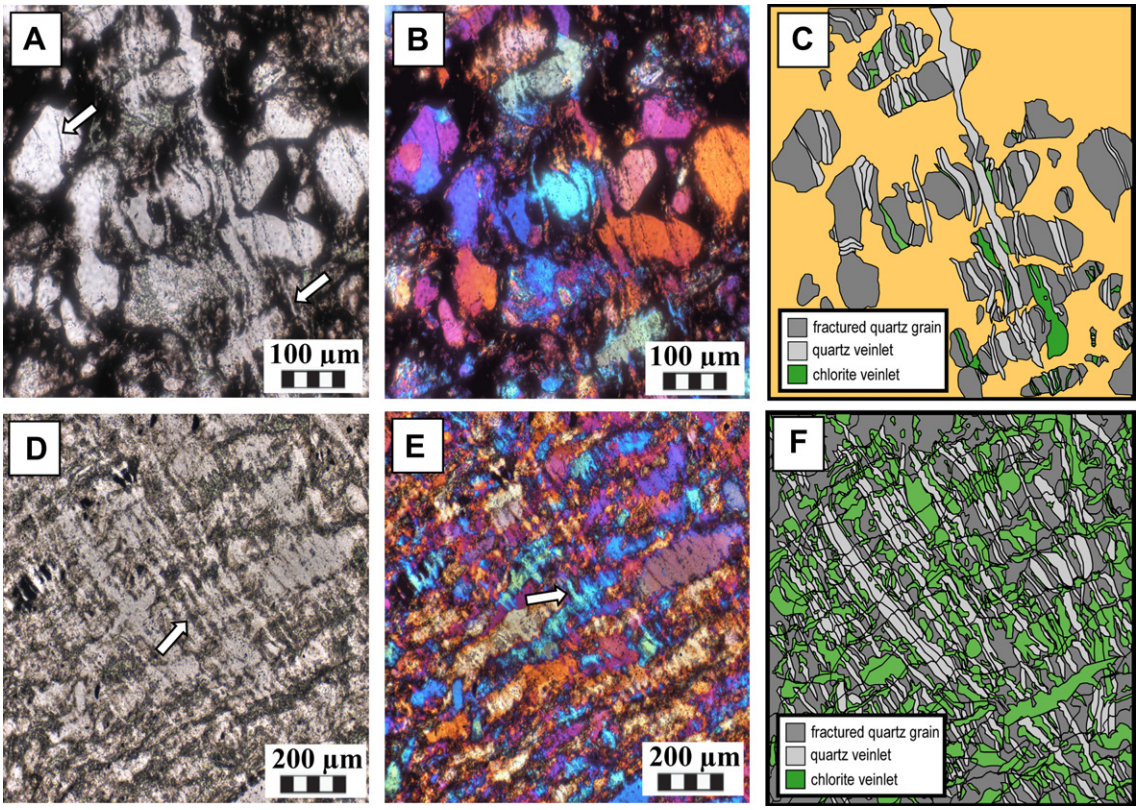

Fig. 4. A) Micrograph (ppl) showing individual quartz grains sealed by quartz veinlets (right arrow), as indicated by thin fluid inclusion bands (left arrow). B) Note that veinlets generally have the same crystallographic orientation as the fractured grains (xpl + gypsum plate). C) Schematic illustration of Fig. 4A/B demonstrating the distribution of grain fragments and veinlets. Many grains show veinlets, which lign-up across several grains in the central part. D) Micrograph (ppl) of bundles of veinlets crossing several fractured grains. Note that the location of veinlet bundles is located closer to the vein as figure a,b. Locally the green-colored chlorite grew faster and overgrew quartz (arrow). E) Same micrograph as d) (xpl + gypsum plate). In contrast to Fig. 4A–C growth competition of vein quartz minerals is clearly visible with overgrowth of neighboring crystals, resulting in serrated grain boundaries. Note that multiple veinlets transect a single host rock grain. Overall, the crystallographic orientation of the vein microstructure is still random. However, the quartz grains oriented with their fastest crystallographic orientation being normal to the vein wall (blue crystals – arrow) start to become dominant. F) Schematic illustration of Fig. 4D/E demonstrating the bi-mineralic sealing of non-localized fractured quartz grains, which mainly lign-up across several grains. Locally growth competition of quartz and chlorite results in either wider quartz or chlorite veinlets.

the serrated grain boundary. If the wall rock contains chlorite, then there is also some chlorite grown into the microfractures (Fig. 4A,D,F). Every veinlet contains bands of fluid inclusions parallel to the fracture wall, in contrast to the host rock grains. Bundles of healed microfractures develop into a single vein where quartz fibers connect fractured host rock grains on either side of the vein (see also Cervantes and Wiltschko, 2005, 2010). Growth competition of quartz veins becomes more pronounced in the bundled zone close to the vein tip (Fig. 4D–F), and fully develops towards a crystallographic preferred orientation in the vein (Fig. 5B). Here, the fastest growing quartz grains (blue in Fig. 5B) are interpreted to overgrow quartz grains with other crystallographic orientations. The vein fibers can become more than 20 times longer than the original grains (Fig. 5A,B). The boundaries of the vein fibers

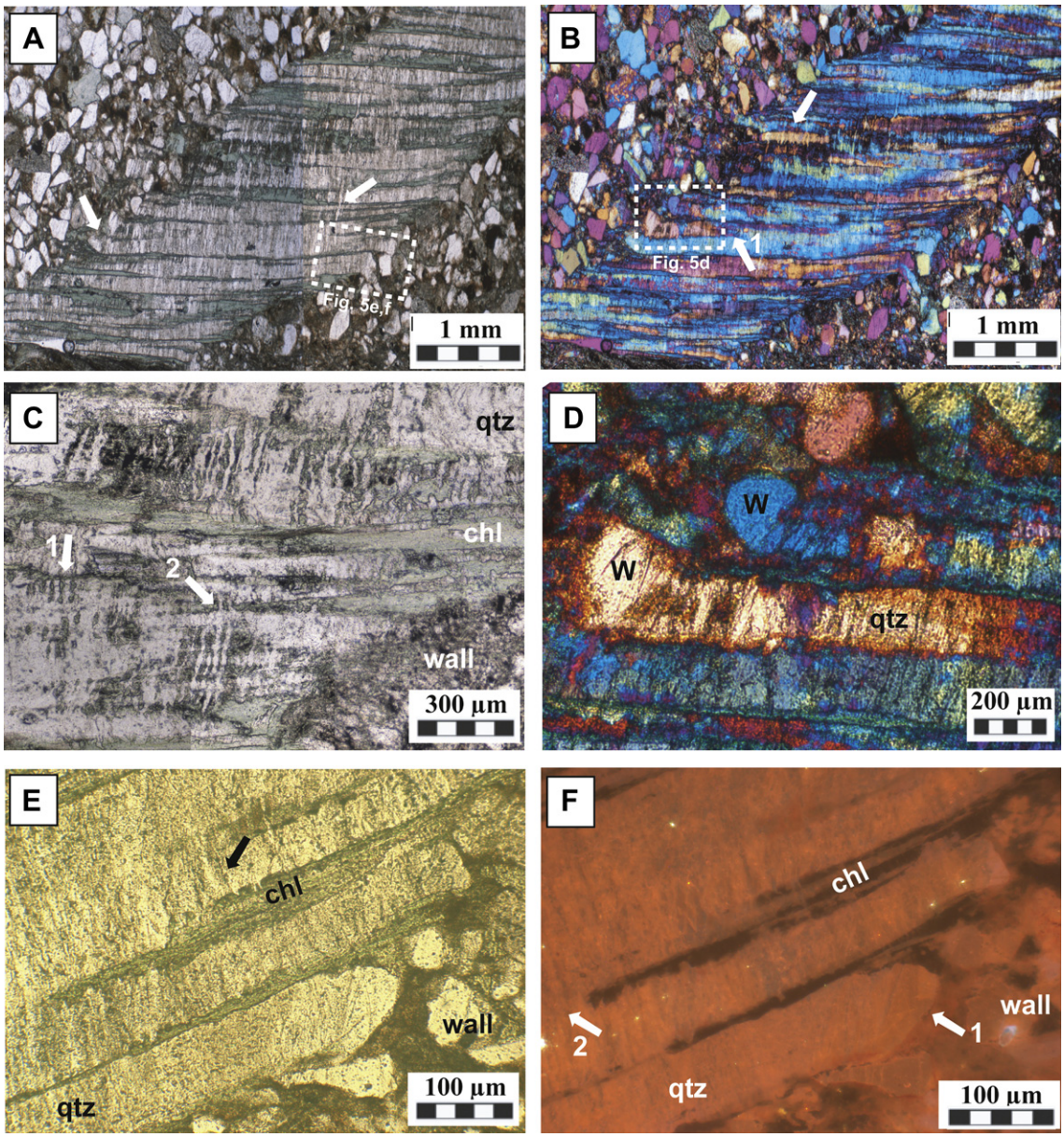

Fig. 5. A) Photograph of a high-angle dilational vein with fibrous appearance. Fractured quartz grains are visible in the wall rock on both sides of vein (left arrow). The fiber–fiber boundaries between quartz–quartz and quartz–chlorite fibers are serrated. Right arrow points to a quartz veinlet which cross-cuts chlorite and quartz fibers and thus indicates cracking within the vein. Box outlines the area covered by Fig. 5E,F. B) Same picture as Fig. 5A, but crossed polarizers plus gypsum plate. The different colors of quartz minerals in the wall rock show that the crystallographic orientation is random. Note that the quartz fibers start to grow into the vein with different crystallographic orientation close the wall rock (1), whereas the crystallographic orientation of quartz fibers in the center of the vein is parallel to the fast growing c-axis (blue color). This indicates significant growth competition between the quartz crystals. Box outlines the area covered by Fig. 5D. C) Detail of high-angle dilational jog veins showing quartz and chlorite fibers. Note areas of chlorite inclusions (1) and quartz veinlets (2). d) Detailed micrograph (xpl + gypsum plate) of Fig. 5B showing the wall–vein interface. The quartz fibers of the vein grew nearly with the same crystallographic orientation as the broken grains of the host rock. e) Detailed micrograph (ppl) of Fig. 5A showing the wall–vein interface of a high-angle dilational jog vein. Notice that fractured quartz grains were sealed by quartz, whereas fractured chlorite grains were preferentially sealed by chlorite. The crack-seal growth path is clearly indicated by fluid inclusion bands in the quartz fibers (arrow). f) Cathodoluminescence image of Fig. 5E at the interface between vein and wall. Note the quartz grain in the wall rock (1) was fractured and overgrown by quartz fiber. Different luminescence colors within a single quartz fiber indicate a variation of the fluid composition at different crack-seal increments, but cannot be linked across two neighboring fibers. Note that lattice disturbances due to variations in dislocation density or style, or to point defect density, distribution or occupancy could also cause different CL properties (Holt and Odgen, 1976). Locally quartz overgrows chlorite (2). (For interpretation of the references to color in this figure legend, the reader is referred to the web version of this article).

commonly have a sawtooth shape, (Ramsay, 1980; Cox and Etheridge, 1983).

4.2.2. High-angle dilational jog veins

High-angle dilational jog veins show two important microstructural elements: (i) vein fibers of quartz and chlorite oriented normal to sub-parallel to the vein wall of dilational jogs (Figs. 3A–D and 5A,B) and (ii) solid and fluid inclusion bands sub-normal to the crystal fibers (Fig. 3C,D). The fibers are optically continuous and connect fractured wall rock grains (Fig. 5A,B,D). Growth competition of neighboring quartz grains results in an overall vein fabric where the fast growing c-axis of the vein fibers is oriented parallel to the fiber boundary. Similar to the bundles of veinlets, the boundaries between these elongated quartz crystals are commonly serrated and irregular.

There are different types of inclusion bands and trails in high-angle veins, consisting of quartz, chlorite, fluid inclusions or wall rock fragments. Close to cleavage domains in the wall rock the veins contain many chlorite crystals oriented parallel to the quartz fibers (Fig. 5A,E). In these chlorite rich zones, chlorite fibers may

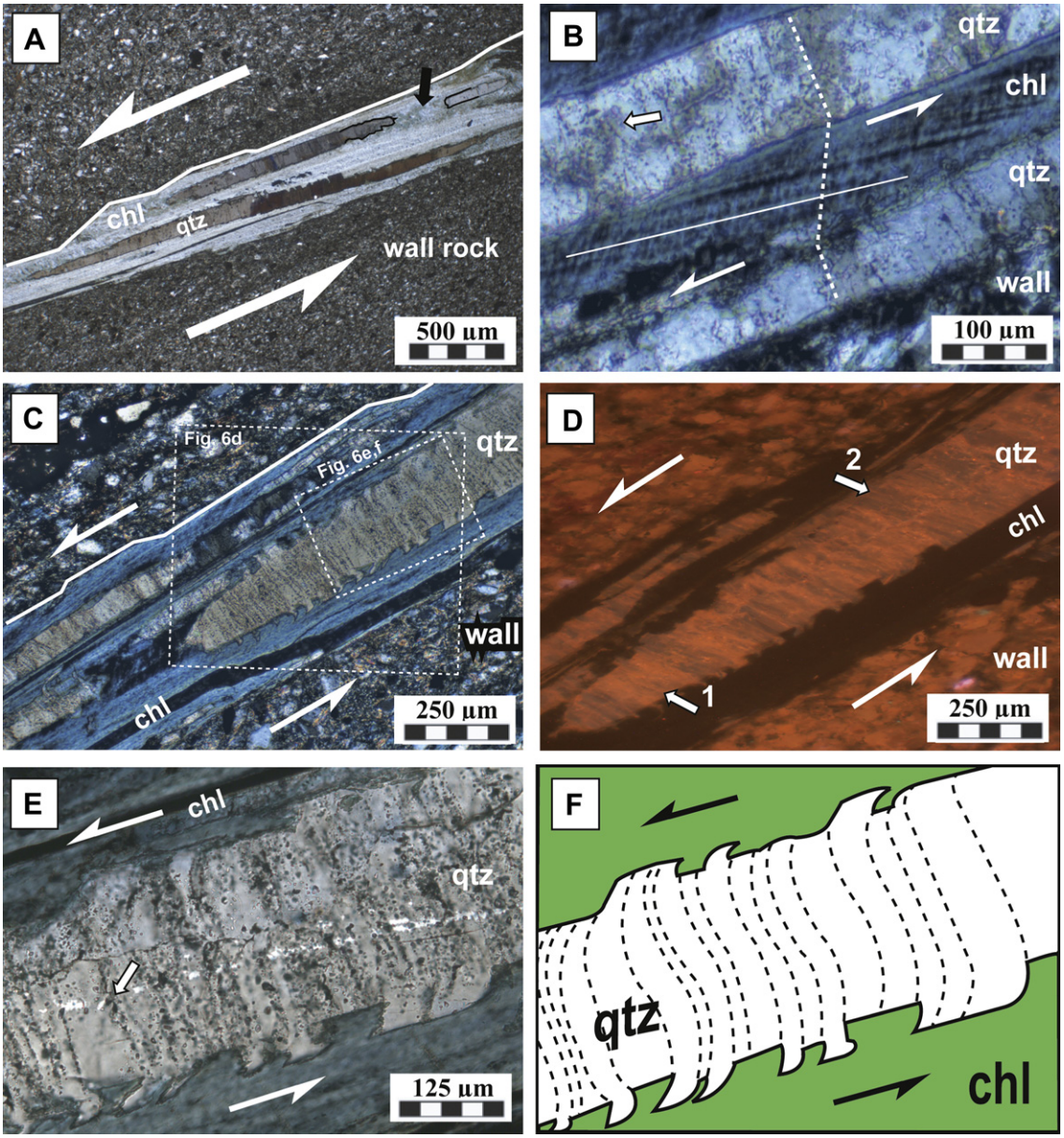

Fig. 6. A) Detail of vein microstructures in the thin low-angle extensional shear vein shown in Fig. 3C, with fractured quartz ribbons separated by chlorite minerals (see black arrow). b) Magnification of Fig. 3D showing oblique crack-seal increments in chlorite and vertical increments in the quartz (dotted lines). Note the traces (solid lines) of the chlorite 001-planes being oblique to the quartz fiber grain boundaries. Shearing inside the vein is further supported by the partially undulose extinction of the quartz ribbons (white arrow). C) Overview micrograph of quartz ribbons in a low-angle extensional shear vein showing fin microstructures on both sides of the ribbon. A magnification of this microstructure is shown in Fig. 6E/F. Second box indicate the area covered in Fig. 6D. D) Cathodoluminescence image of C). Quartz ribbons show orange (1) and purple (2) stripes normal to quartz ribbon indicating that the fluid precipitating quartz could have different trace element compositions during incremental crack-sealing. E) Detailed micrograph of a quartz ribbon with fin microstructure as shown in Fig. 6C. The quartz ribbon shows curved fin-shaped quartz on both sides of the quartz ribbons, tapering off in the adjacent chlorite fibers. The quartz ribbon shows numerous fluid inclusion bands normal to the fiber grain boundaries (white arrow). F) Schematic illustration of the fin microstructure shown in Fig. 6E. The crack-seal increments are indicated by fluid inclusion bands (dotted lines). (For interpretation of the references to color in this figure legend, the reader is referred to the web version of this article).

continue across the vein, or may be separated by individual, 10–20 μm wide crack-seal bands of quartz. The quartz crack-seal bands may cross several of these elongated vein crystals (both quartz and chlorite) (Fig. 5C), and display microfractures healed by quartz at the expense of chlorite. If the wall rock is dominated by quartz, chlorite appears as inclusion bands within crack-sealed quartz crystals (Fig. 5A–C). Thus, vein fibers of quartz and chlorite are dominantly quartz and chlorite sealed microfractures, respectively. However, one mineral phase can be overgrow the neighboring second mineral phase, fragmenting the elongated crystal (Fig. 5A–C).

Inclusion bands may also consists of wall rock lithons (Fig. 3C,D). These wall rock inclusion bands are interpreted to represent repeated crack-seal events in the wall rock, or by the coalescence of a bundle of veinlets into one large vein (Cervantes and Wiltschko, 2005, 2010).

4.2.3. Low-angle extensional shear veins

The low-angle extensional shear veins have different microstructures as compared to the high-angle dilational jogs, which also consist of quartz and chlorite fibers. The most striking microstructural element in such low-angle extensional shear veins are quartz ribbons which are fin-shaped on both sides (Fig. 6A,C–F). These quartz ribbons orientated sub-parallel to the vein wall have a diameter of around 200 mm and are often surrounded by chlorite.

The amplitude of the fin microstructures into the neighboring chlorite grains is reasonably constant at 10 μm. Commonly there is a clear relationship between the fin microstructures and the fluid inclusions trails inside the quartz ribbons (Fig. 6C,E,F). Often the quartz ribbons show undulose extinction and in a few cases incipient recrystallization (Fig. 6B). In a number of cases the long quartz ribbons shows angular to rounded ends (e.g. Fig. 6A) and are surrounded by chlorite. The angular ends of the quartz ribbons are oriented parallel to their crack-seal bands (and are oriented subnormal to the vein wall), which were sealed with chlorite. The chlorite between quartz ribbons has a strong preferred orientation and a well developed foliation with a number of sheared crack-seal bands (Fig. 6B).

Overall, microstructures of both quartz and chlorite suggest that the low-angle extensional shear veins have been strongly sheared. We interpret this to point to ductile deformation producing sheared chlorites between plastically deformed quartz ribbons, and incipient recrystallization of quartz ribbons.

5. Simulation of vein microstructures

The detailed description of bi-mineralic crack-seal veins analyzed during this study has shown a variety of microstructures which have not been described in previous studies paying most attention on mono-mineralic veins. The following simulations aim to explain the formation of (1) serrated grain boundaries in bi-mineralic veins and (2) fin microstructures.

5.1. Growth rates in polyphase veins

The kinematics of crystal growth in bi-mineralic veins is undoubtedly very complex, depending on local differences in

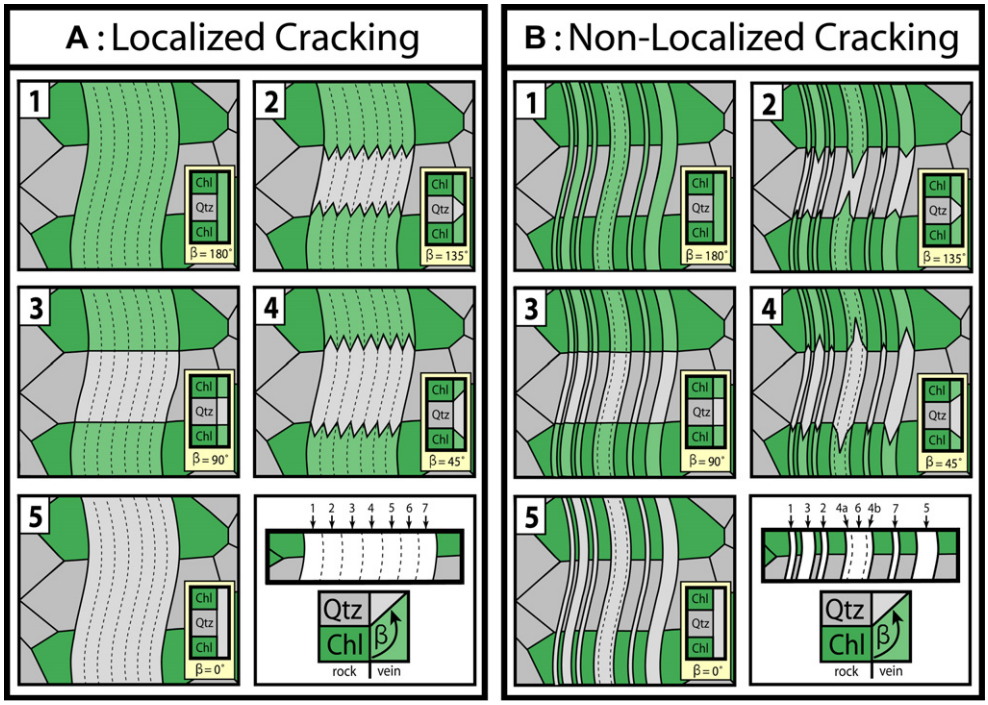

Fig. 7. Series of 2D geometric simulations for a vein formed by localized cracking in the vein and non-localized cracking within the wall rock using different values of growth anisotropy angle (β): v = growth velocities (1) $v_{quartz} << v_{chlorite}$, (2) $v_{quartz} < v_{chlorite}$, (3) $v_{quartz} = v_{chlorite}$, (4) $v_{quartz} > v_{chlorite}$, (5) $v_{quartz} >> v_{chlorite}$. Dark colors represent grains of the host rock, light colors represent veins. a) Localized cracking results in mono-mineralic veins, if the growth rate of the first mineral phase is significantly higher than the second mineral phase (1 and 5). Overall, the mineral phase with the fast growth rate normal to the fracture prevails. Note that the growth anisotropy results in serrated (sawtooth-) grain boundaries in 2 and 4, while a fibrous microstructure form when growth rates of the two mineral phases are similar (3). Serrated grain boundaries are thus a result of anisotropic growth. B) Variation in growth rates (1–6) is the same as in Fig. 7A for non-localized cracking. Again, serrated grain boundaries form in 2 and 4. In contrast to the localized cracking model, the final microstructure of 2 and 4 consists of an arrangement of newly grown minerals and host rock fragments. It will be difficult to distinguish localized and delocalized vein microstructures if fracture spacing is close. If only one mineral phase grows (1 and 5), the overall final vein microstructure consists of veinlets and host rock fragments of the other mineral phase. If fracture spacing is close, such host rock fragments can easily be misinterpreted as inclusion trails.

mineral saturation, diffusive or advective transport mechanisms, and the local growth factors such as crystal orientation and development of crystal facets. In mono-mineralic polycrystals some basic principles were formulated by Mügge (1928), Schmidegg (1928), Grigor'ev (1965) and more recently further developed by others (Urai et al., 1991; Thijssen et al., 1992; Bons, 2001; Hilgers and Urai, 2002; Nollet et al., 2005 or Hubert et al., 2009).

In the simplest case of an irrational growth surface between two crystals in a mono-mineralic vein, Urai et al. (1991) argued that the two crystals will display isotropic growth during the initial phases of epitaxial growth before the development of facets, and that this state is restored after each crack-event. In an experimental study Nollet et al. (2005) measured the critical growth distance for a rounded crystal to develop facets as 12–18 μm depending on the supersaturation of the solution, which can be interpreted as the critical distance at which growth changes from isotropic to anisotropic growth.

In this paper we make the simple assumption that the two mineral phases display the same isotropic growth as for a single phase, but at different growth rates due to differences in supersaturation of the two phases. This will lead to different propagation directions of the grain boundary between two mineral phases with respect to the local fracture surface. Here we define the growth anisotropy as angle β as the angle between the propagation directions of the phase boundary and the local fracture surface (inlets Fig. 7A,B). For $\beta = 0^\circ$ the vein will be completely quartz-filled (Fig. 7A 5 and B 5) and for $\beta = 180^\circ$ the vein will be completely chlorite-filled (Fig. 7A 1 and B 1); for $\beta = 90^\circ$ the grain boundary will propagate perpendicular to the local fracture surface (Fig. 7A 3 and B 3). For other values of β the grain boundary propagates in an oblique direction (Fig. 7A 2,4 and B 2,4).

In what follows, we present simple, 2D simulations of the evolving microstructure in this system. For the simulations with localized cracking the sealed microfractures were always broken at the same position directly at the interface of vein and host rock (inlet Fig. 7A). In this series we kept the width of each microfracture the same. Results clearly reflect the effect of β, with a pure quartz vein for $\beta = 0^\circ$ (Fig. 7A 5), quartz–chlorite fibers with serrated grain boundaries and chlorite fibers thinner than the broken grain in the host rock for $\beta = 45^\circ$ (Fig. 7A 4), quartz–chlorite fibers with straight boundaries and fibers the same size as the broken grain in the host rock for $\beta = 90^\circ$ (Fig. 7A 3), quartz–chlorite fibers with serrated grain boundaries and quartz fibers thinner than the broken grain in the host rock for $\beta = 135^\circ$ (Fig. 7A 2), and a pure chlorite vein for $\beta = 0^\circ$ (Fig. 7A 1). Fibers with serrated grain boundaries evolve for $\beta \neq 0^\circ$, $\beta \neq 90^\circ$ and $\beta \neq 180^\circ$ (Fig. 7A 2,4).

In Fig. 7B we used the same range of β, but with non-localized cracking taking place both in the vein and the wall rock (inlet Fig. 7B). Overall, simulations with non-localized cracking do not differ from localized cracking with exception of the more regular appearance of the localized cracking (Fig. 7A 2–4 and B 2–4). The most significant differences appear in the simulations for localized and non-localized cracking using $\beta = 0^\circ$ and $\beta = 180^\circ$ (Fig. 7A 1,5 and B 1,5). Here, the final veins grown during non-localized cracking contain several solid host rock inclusions of the second mineral phase, because numerous microfractures broke the wall rock grains in several parts. Furthermore, the non-localized cracking (Fig. 7B) of this series has many similarities with the bundles of incipient veinlets shown in Fig. 4D–F.

The model also shows the formation of serrated grain boundaries between two mineral phases at different growth rates of quartz and chlorite for both the localized and the non-localized cracking model. If the quartz grows faster than the chlorite (Fig. 7A 4, B 4), serrated grain boundaries of quartz crystals will intrude into the chlorite crystals. The vein grain boundaries becomes more serrated at greater crack-seal increments as shown Fig. 8, where we assumed a constant anisotropic growth ($\beta = 45^\circ$), but different opening width of the localized microfractures (Fig. 8). This is similar to the microstructures observed on the high-angle dilational jog veins (Fig. 5A,B).

6. Discussion

All quartz–chlorite veins clearly show shear indicators and are dominantly found within fault zones. Based on their geometry, they are interpreted as shear veins.

6.1. Crack-seal vein models and inclusion arrangement

6.1.1. Evolution from individual cracked grains to fully developed veins

Our veins show crack-seal microstructures both within the vein and in the host rock near the vein's tip. Veinlets form in cracked and re-sealed grains in the host rock, and become progressively longer (but not thicker) and cross multiple grains. This variation from individual veinlets towards bundled veinlets reflects progressive brittle deformation, during the initial vein formation by non-localized cracking. Microfracturing becomes more localized in the veins, resulting finally in a fully developed vein microstructure (see also Cervantes and Wiltschko, 2005, 2010).

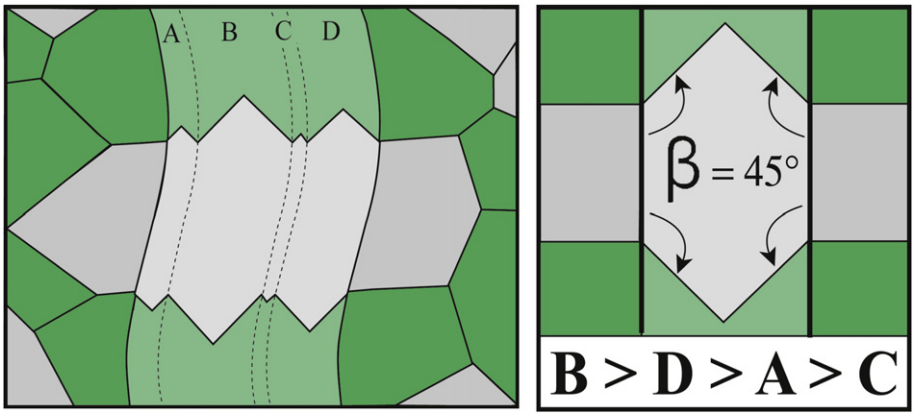

Fig. 8. Serrated grain boundaries form during anisotropic growth of two adjacent vein crystals as illustrated by localized cracking with different opening widths at constant $\beta = 45^\circ$. Four different opening widths were simulated, showing that the vein grain boundary becomes more serrated at greater crack-seal increments.

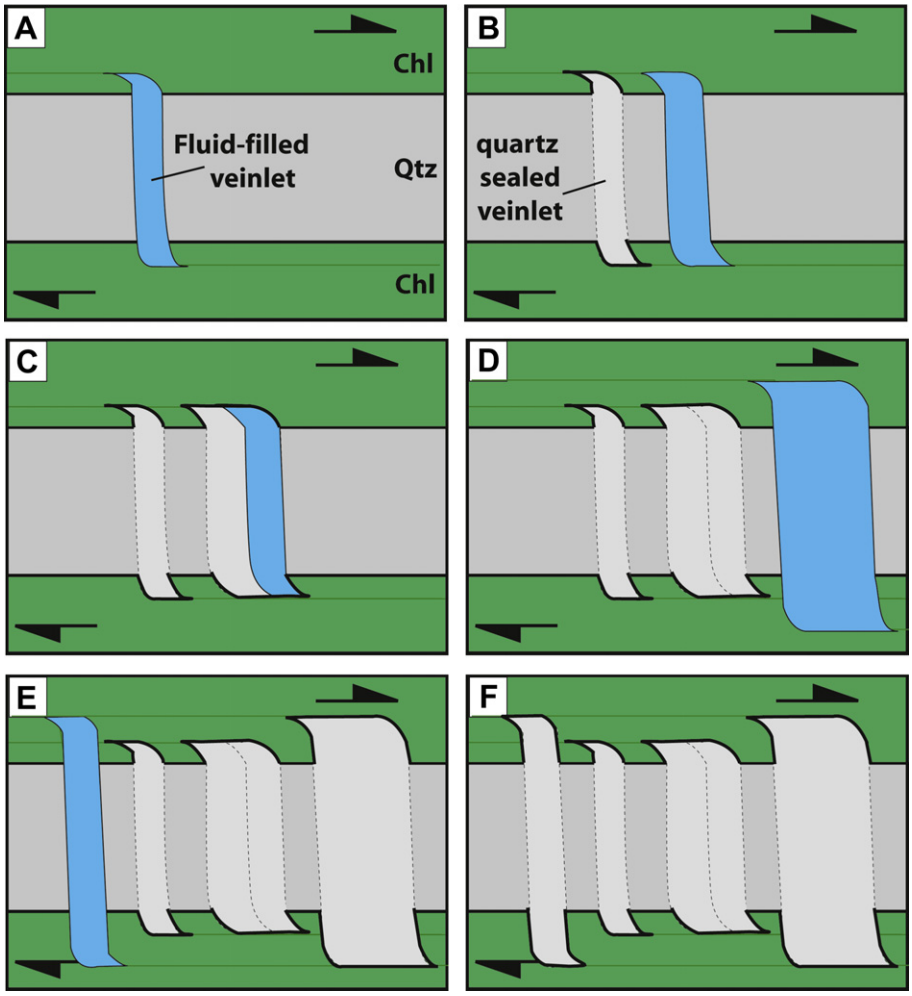

Fig. 9. Simulation of fin-shape quartz microstructure in quartz ribbons, named fin microstructure (compare with Fig. 6C–F). Microfractures form in quartz ribbons during ongoing shear and taper off in the neighboring chlorite minerals. Note that the neighboring quartz curves are parallel to each other and thus do not show any difference in shear deformation.

Sindern et al. (2007, 2008), based on geochemical analyses, proposed that fluid flow occurred during Variscan orogeny with fluid flow along faults lasting less than 10,000 years, which would constrain the duration of our bi-mineralic crack-seal vein formation. Hundreds to thousands of crack-seal events present in our veins would imply that a veinlet is sealed within less than a few years. Several authors propose that both episodic (microseismic) slip, or nearly continuous aseismic fault creep could form crack-seal veinlets, the difference being the rapid vs. continuous opening (Gaviglio, 1986; Davison, 1995; Lee and Wiltschko, 2000). The fibers of our veins with approximately 10 μm wide crack-seal increments can be explained by both mechanisms, because the width of the crack-seal increments is within the maximum growth distance of 10–20 μm required for the formation of fibrous microstructures (Hilgers et al., 2001; Nollet et al., 2006). Also, the timescale deduced above would match with the recurrence time found in microseismicity around active faults (e.g. Tsukuda, 1985). Thus the veinlets forming crack-seal veins could represent microseismic events.

The microfractures are healed by epitaxial growth either by quartz or by chlorite, depending on the mineralogy of the fractured grains. Where quartz grows faster than the chlorite, it will also grow into the space between the fractured chlorite, producing the characteristic serrated microstructure, and vice versa (Figs. 5A–C, 7a and b). Overall the displacement-tracking capability of such serrated grain boundary is poor. End-members are mono-mineralic veins, where all the microfractures were completely healed by either chlorite or by quartz. If the quartz- and chlorite-growth rate is equal, the grain boundary can be straight across the vein or contain a step due to the shear component of opening (Fig. 7A3, B3; cf. Fig. 9 of Urai et al., 1991). Such veins consist of both mineral phases and are thus bi-mineralic.

Cohesion between the healed vein and wall must have been high so that new veinlets formed in the host rock and incorporated lithons during ongoing growth (Holland and Urai, 2010). The veinlets in the fibers suggest that microfracturing did not only occur in the wall rock but also in the veins themselves. Reasons for this can be incomplete sealing of a microfracture before the next fracturing event or the low tensile strength of a healed quartz–chlorite boundary as compared to a healed quartz–quartz boundary (Laubach, 1988; Laubach et al., 2004a; Holland and Urai, 2010).

By progressive crack-seal processes the grains evolve into fibers in the high-angle dilational jog veins and into the quartz ribbons with fins in the low-angle extensional shear vein. Since all fins are curved into the same direction on one side of the quartz ribbons and towards the opposing direction on the other side, we rule out post-vein formation. Since they are the prolongation of quartz from a single crack-seal band in the quartz ribbon into the surrounding chlorite vein, they are related to the crack-seal vein

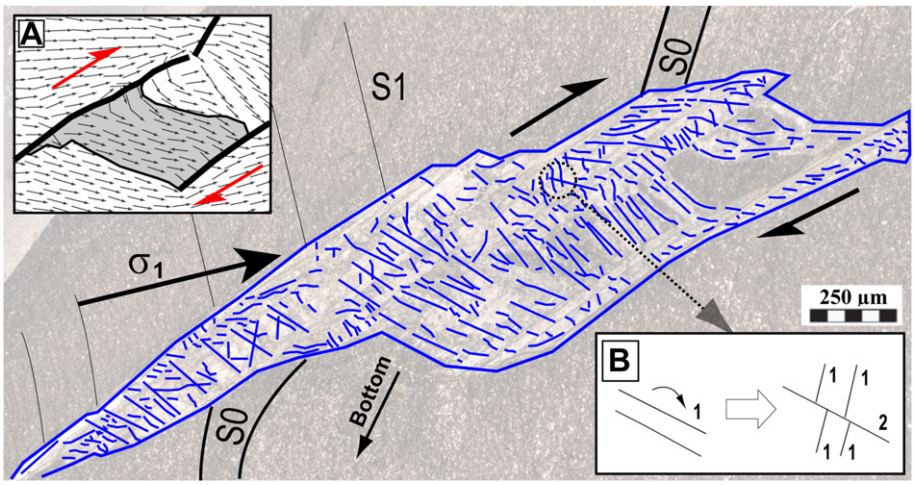

Fig. 10. Trace of crack-seal veinlet orientations within shear vein with a dilational jog vein in the center and extensional shear vein at the lower left. The veinlets become gradually inclined towards the wall rock with an overall sigmoidal shape, which may be a result of shear or an alignment parallel to the local principal stress (see text for discussion). Insert A shows the orientation of local principal stresses in a dilational jog vein (after Soliva et al., 2010), which matches well with the orientation of veinlets in the shear vein. Note that the vein locally exposes two generations of veinlets (insert B), which represents a later stage of mineralization.

formation. The evolution of the fin microstructures in quartz ribbons in the low-angle extensional shear veins is interpreted to have formed in small (crack-seal) pull-aparts formed during ongoing deformation of the low-angle extensional shear vein (Fig. 9). The shear direction deduced from the micro-tension gashes within the quartz ribbons coincides with the shear direction of the vein (Figs. 6C–F and 9). We propose that such fin microstructures are diagnostic in bi-mineralic low-angle shear veins at regional settings.

We interpret the high-angle dilational jog veins to represent sites where a large number of veinlets formed in close vicinity to each other (see also Gaviglio, 1986; Labaume et al., 1991; Lee and Wiltschko, 2000; Cervantes and Wiltschko, 2005, 2010; Holland and Urai, 2010), in a prolonged deformation phase under crack-seal conditions.

6.1.2. Inclusion arrangements

Host rocks lithons clearly indicate non-localized cracking in the host rock, while differently oriented veinlets within the vein indicate different microfracturing events during progressive shearing and vein formation (Fig. 3C,D).

Many studies showed that inclusions bands are arranged normal to the opening trajectory of dilational jogs (Cox and Etheridge, 1983; Gaviglio, 1986; Cox, 1987; Lee and Wiltschko, 2000). Koehn and Passchier (2000) proposed three models with different opening directions to explain the shape of the vein and the orientation of the inclusion bands and trails. In that model our crack-seal veins should be classified as oblique opening-type veins, because they show clear bedding offset and no jog parallel opening (Fig. 3B,C). However, the RWTH-1 crack-seal veins contain typical inclusion bands and inclusion trails that do not match with the classification outlined above (Figs. 3C,D or 5C). Therefore we suggest to extend the classification of Koehn and Passchier (2000).

6.2. Stress orientation

In many studies the orientation of stress trajectories around shear zones and dilational jog veins were deduced from numerical modeling and photoelasticity experiments (Ohlmacher and Aydin, 1997; Connolly and Cosgrove, 1999; Fletcher and Pollard, 1999; Salvini et al., 1999; Nemcok et al., 2002; de Joussineau et al., 2003; Soliva et al., 2010). However, we are not aware that these results were compared to the crack-seal microstructure patterns within a natural vein. Fractures and veinlets are a useful tool to infer on stress orientation inside a crack-seal vein, assuming that the

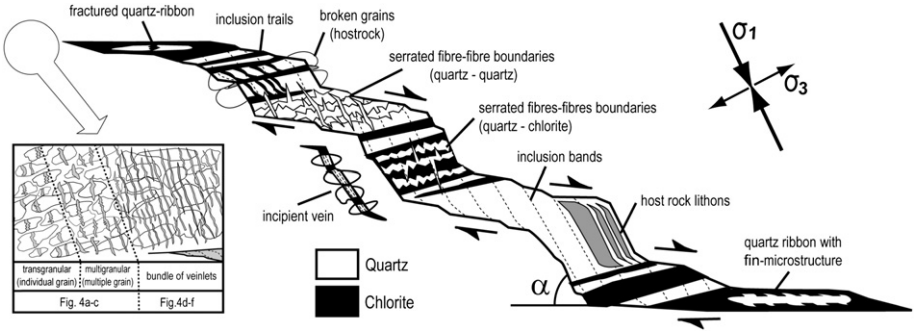

Fig. 11. Overview of microstructures observed in our bi-mineralic veins. The vein illustrated here consists of three thick, high-angle dilational jog veins in the central part which continue as thinner low-angle extensional shear veins on both sides of the vein. The orientation of crack-seal veinlets is constant across the overall microstructure, but shows a sigmoidal shape which may display the variation of the local stress orientation across the vein. Lithons point to non-localized cracking in the host rock, while serrated quartz–chlorite fibers imply a more localized cracking in the vein and anisotropic growth. Note the fin microstructure indicating shear in quartz ribbons. Box on the left shows the initial stages in the evolution of the veins. Veins start as transgranular fractures within individual quartz grains successively crossing multiple grains and evolving towards bundles of multiple veinlets, resulting in a vein microstructure. Thin incipient veins oriented can also be observed parallel to the high-angle dilational jog vein.

veinlets are orientated normal to the local minimum principal stress.

Fig. 10 shows that the mapped veinlets inside a high-angle dilational jog fit well with the principal stress trajectories modeled numerically (e.g. Ohlmacher and Aydin, 1997; Soliva et al., 2010). The veinlets inside a dilational jog vein are orientated at high-angle to the wall rock, towards the shear planes at the margin of the vein the veinlets are orientated at a lower angle (Fig. 11). Since the microstructures of the veinlets show no increase in deformation intensity towards the wall rock, it is suggested that they may thus trace the stress orientation within the dilational jog.

7. Conclusions

Syntectonic bi-mineralic quartz–chlorite veins show a crack-seal pattern of ataxial type microstructures. The overall vein geometry consists of a high-angle dilational jog vein in the center with fibers oriented normal to the vein wall, and evolves towards a low-angle shear vein on the sides with quartz ribbons oriented sub-parallel to the vein wall. The most characteristic microstructures of the high-angle dilational jog are solid and fluid inclusion bands/trails as well as serrated fiber boundaries, whereas the low-angle shear veins contain fin microstructures. These previously unrecognized microstructure are fin-shaped quartz ribbons surrounded by chlorite and found in the low-angle extensional shear veins. Fin microstructures may form by repeated cracking and sealing during shear along the quartz–chlorite boundary.

Veinlets inside a high-angle dilation jog fit well with principal stress trajectories. Assuming that their orientation is normal to the minimum stress they are a useful tool to track the stress orientation within dilational jog veins.

Overall the observed quartz–chlorite crack-seal veins show a transition from non-localized veinlets in single grains towards a bundle of veinlets in the host rock. Such bundles of veinlets may further evolve into a vein.

Simple 2D simulations of the evolution of microstructure in two-phase crack-seal veins reproduce most observed microstructures quite well. The angle of shear (α) and the angle of growth anisotropy (β) control the overall microstructure and determine whether a quartz or chlorite microfabric prevails. Factors controlling the vein microstructure are the width of the crack increments and the growth anisotropy, which generally forms serrated grain boundaries due to growth competition of neighboring grains unless the growth anisotropy β is $\neq 0^\circ, 90^\circ, 180^\circ$. Both localized and non-localized cracking forms similar vein patterns with serrated grain boundaries. Host rock fragments will be included into the vein during non-localized cracking. The tracking capability of the serrated fiber boundaries is poor.

Acknowledgments

The German Science Foundation (DFG) is thanked for financial support of the “RWTH-1” project. The authors are grateful to Katerina Scholz, Maria Chatziliadou und Markus Lögering for providing their thin sections and supporting material. Ute Trautwein-Bruns and Sven Sindern are thanked for discussions and providing material. We also would like to thank Werner Kraus, Thomas Derichs, Brigitte Wienen and Philipp Binger for thin section preparation. Special thanks to Uwe Wollenberg for XRD-measurements and assistance during SEM and CL-studies. We wish to thank Shaun Barker, an anonymous reviewer and Tom Blenkinsop for their thorough reviews and constructive comments.

References

Becker, S., 2008. The Aachen fold and thrust belt: an integration of surface geology, reflection seismics and new subsurface data of the well RWTH-1. Diploma Thesis, RWTH Aachen University.
Behr, H.J., Horn, E.E., Frentzelbeyme, K., Reutel, C., 1987. Fluid inclusion characteristics of the Variscan and post-Variscan mineralizing fluids in the Federal Republic of Germany. Chemical Geology 61, 273–285.
Blundell, D.J., Freeman, R., Mueller, S., Button, S., 1992. A Continent Revealed: The European Geotraverse. Cambridge University Press, Cambridge.
Bons, P.D., Jessell, M.W., 1997. Experimental simulation of the formation of fibrous veins by localised dissolution-precipitation creep. Mineralogical Magazine 61, 53–63.
Bons, P.D., 2000. The formation of veins and their microstructures. In: Jessell, M.W., Urai, J.L. (Eds.), Stress, Strain and Structure: a volume in honour of Win D. Means. Journal of Virtual Explorer 2.
Bons, P.D., 2001. Development of crystal morphology during unitaxial growth in a progressivley widening vein: I. The numerical model. Journal of Structural Geology 23, 865–872.
Cervantes, P., Wiltschko, D.V., 2005. A Model for Syntectonic Fibrous Vein Growth Inferred from Microtextures. Ouachitas Orogen, Arkansas. American Geophysical Union, San Francisco. Fall Meeting 2005.
Cervantes, P., Wiltschko, D.V., 2010. Tip to mid-point observations on syntectonic veins, Ouachita orogen, Arkansas: trading space for time. Journal of Structural Geology 32, 1085–1100.
Chatziliadou, M., 2009. Rb-Sr Alter und Sr–Pb Isotopencharakteristik von Gangmineralisationen in paläozoischen Gesteinen am Nordrand des linksrheinischen Schiefergebirges (Raum Stolberg-Aachen-Kelmis) und Vergleich mit den rezenten Thermalwässern von Aachen-Burtscheid. Ph.D. Thesis, RWTH Aachen University.
Connolly, P., Cosgrove, J., 1999. Prediction of fracture-induced permeability and fluid flow in the crust using experimental stress data. AAPG Bulletin 83, 757–777.
Cox, S.F., Etheridge, M.A., 1983. Crack-seal fiber growth mechanisms and their significance in the development of oriented layer silicate microstructures. Tectonophysics 92, 147–170.
Cox, S.F., 1987. Antitaxial crack-seal vein microstuctures and their relationship to displacement paths. Journal of Structural Geology 9, 779–787.
de Joussineau, G., Petit, J.P., Gauthier, B.D.M., 2003. Photoelastic and numerical investigation of stress distributions around fault models under biaxial compressive loading conditions. Tectonophysics 363, 19–43.
de Vos, W., Verniers, J., Herbosch, A., Vanguestaine, M., 1993. A new geological map of the Brabant Massif, Belgium. Geological Magazine 130, 605–611.
Davison, I., 1995. Fault slip evolution determined from crack-seal veins in pull-aparts and their implications for general slip model. Journal of Structural Geology 17, 1025–1034.
Demoulin, A., Hallot, E., 2009. Shape and amount of the Quaternary uplift of the western Rhenish shield and the Ardennes (western Europe). Tectonophysics 474, 696–708.
Dietrich, D., Grant, P.R., 1985. Cathodoluminescence petrography of syntectonic quartz fibers. Journal of Structural Geology 7, 541–553.
Durney, D.W., Ramsay, J.G., 1973. Incremental strains measured by syntectonic crystal growth. In: Jong, K.A., Scholten, R. (Eds.), Gravity and Tectonics. Wiley, New York, pp. 67–96.
Fielitz, W., Mansy, J.L., 1999. Pre- and synorogenic burial metamorphism in the Ardenne and neighboring areas (Rhenohercynian zone, central European Variscides). Tectonophysics 309, 227–256.
Fielitz, W., 1992. Variscan transpressive inversion in the northwestern central Rhenohercynian belt of western Germany. Journal of Structural Geology 14, 547–563.
Fisher, D.M., Brantley, S.L., 1992. Models of quartz overgrowth and vein formation: deformation and episodic fluid flow in an ancient subduction zone. Journal of Geophysical Research 97, 20043–20061.
Fletcher, R.C., Pollard, D.D., 1999. Can we understand structural and tectonic processes and their products without appeal to a complete mechanism? Journal of Structural Geology 21, 1071–1088.
Garcia-Castellanos, D., Cloething, S., van Balen, R., 2000. Modelling the middle Pleistocene uplift in the Ardennes-Rhenish Massif: thermo-mechanical weakening under the Eifel? Global and Planetary Change 27, 39–52.
Gaviglio, P., 1986. Crack-seal mechanism in limestone: a factor of deformation in strike-slip faulting. Tectonophysics 131, 247–255.
Geluk, M.C., Duin, E.J.T., Dusar, M., Rijkers, R.H.B., Vandenberg, M.W., Vanrooijen, P., 1994. Stratigraphy and tectonics of the Roer Valley Graben. Geologie En Mijnbouw 73, 129–141.
Grigor'ev, D.P., 1965. Ontogeny of Minerals. Israel Program for Scientific Translation Ltd., Jerusalem.
Hance, L., Dejonghe, L., Ghysel, P., Laloux, M., Mansy, J.L., 1999. Influence of heterogeneous lithostructural layering on orogenic deformation in the Variscan Front Zone (eastern Belgium). Tectonophysics 309, 161–177.
Hilgers, C., Urai, J.L., 2002. Microstructural observations on natural syntectonic fibrous veins: implications for the growth process. Tectonophysics 352, 257–274.
Hilgers, C., Koehn, D., Bons, P.D., Urai, J.L., 2001. Development of crystal morphology during unitaxial growth in a progressively widening vein: II. Numerical

simulations of the evolution of antitaxial fibrous veins. Journal of Structural Geology 23, 873–885.
Holland, M., Urai, J.L., 2010. Evolution of anastomosing crack-seal vein networks in limestones: insight from an exhumed high-pressure cell, Jabal Shams, Oman Mountains. Journal of Structural Geology 32, 1279–1290.
Hollmann, G., von Winterfeld, C., 1999. Laterale Strukturvariationen eines Vorlandüberschiebungsgürtels. Zeitschrift der Deutschen Geologischen Gesellschaft 150, 431–450.
Hollmann, E.G., 1997. Der Variszische Vorlandüberschiebungsgürtel der Ostbelgischen Ardennen – ein bilanziertes Profil. Ph.D. Thesis, RWTH Aachen University.
Holt, D.B., Odgen, R., 1976. Observation of dislocation in a silicon phototransistor by scanning electron microscopy using the barrier electron voltaic effect. Solid State Electronics 19, 37–40.
Hubert, J., Emmerich, H., Urai, J.L., 2009. Modelling the evolution of vein microstructure with phase-field techniques – a first look. Journal of Metamorphic Geology 27, 523–530.
Koehn, D., Passchier, C.W., 2000. Shear sense indicators in striped bedding-veins. Journal of Structural Geology 22, 1141–1151.
Kooi, H., Johnston, P., Lambeck, K., Smither, C., Molendijk, R., 1998. Geological causes of recent (similar to 100 yr) vertical land movement in the Netherlands. Tectonophysics 299, 297–316.
Kukla, P.A., Mohr, M., Oesterreich, B., Wrede, V., 2002. Erläuterungen zu den Vorprofilen für die geplante Geothermie – Bohrung "Super C" in Aachen. RWTH Aachen University/Geological Survey NRW, Aachen/Krefeld.
Labaume, P., Berty, C., Laurent, P., 1991. Syn-diagenetic evolution of shear structures in superficial nappes – an example from the northern Apennines (NW Italy). Journal of Structural Geology 13, 385–398.
Laubach, S.E., Lander, R.H., Bonnell, L.M., Olson, J.E., Reed, R.M., 2004a. Opening histories of fractures in sandstone. In: Cosgrove, J., Engelder, T. (Eds.), The Initiation, Propagation, and Arrest of Joints and Other Fractures. Geological Society Special Publication, vol. 231, pp. 1–9.
Laubach, S.E., Reed, R.M., Olson, J.E., Lander, R.H., Bonnell, L.M., 2004b. Coevolution of crack-seal texture and fracture porosity in sedimentary rocks: cathodoluminescence observations of regional fractures. Journal of Structural Geology 26, 967–982.
Laubach, S.E., 1988. Subsurface fractures and their relationship to stress history in East Texas Basin sandstone. Tectonophysics 156, 37–49.
Lee, Y.J., Wiltschko, D.V., 2000. Fault controlled sequential vein dilation: competition between slip and precipitation rates in the Austin Chalk, Texas. Journal of Structural Geology 22, 1247–1260.
Lögering, M.J., 2008. Fluid evolution, vein formation and alteration associated with a low angle shear zone at the northern Variscan fold-and-thrust belt in the vicinity of the Aachen Geothermic-drilling, Western Germany. Ph.D. Thesis, RWTH Aachen University.
Milliken, K.L., 2003. Late diagenesis and mass transfer in sandstone-shale sequences. In: Mackenzie, F.T., Holland, H.D., Turekian, K. (Eds.), Treatise in Geochemistry, pp. 159–190.
Muchez, P.H., Sintubin, M., 1998. Contrasting origin of palaeofluids in a strike-slip fault system. Chemical Geology 145, 105–114.
Mügge, O., 1928. Ueber die Entstehung faseriger Minerale und ihrer Aggregationsformen. Neues Jahrbuch für Mineralogie, Geologie und Paläontologie 58, 303–348.
Nemcok, M., Henk, A., Gayer, R.A., Vandycke, S., Hathaway, T.M., 2002. Strike-slip fault bridge fluid pumping mechanism: insights from field-based palaeostress analysis and numerical modelling. Journal of Structural Geology 24, 1885–1901.
Nierhoff, R. 1994. Metamorphose-Entwicklung im Linksrheinischen Schiefergebirge: Metamorphosegrad und-verteilung sowie Metamorphosealter nach K–Ar-Datierungen. Ph.D. Thesis, RWTH Aachen University.
Nollet, S., Urai, J.L., Bons, P.D., Hilgers, C., 2005. Numerical simulations of polycrystal growth in veins. Journal of Structural Geology 27, 217–230.
Nollet, S., Hilgers, C., Urai, J.L., 2006. Experimental study of polycrystal growth from an advecting supersaturated fluid in a model fracture. Geofluids 6, 185–200.
Ohlmacher, G.C., Aydin, A., 1997. Mechanics of vein, fault and solution surface formation in the Appalachian Valley and Ridge, northeastern Tennessee, U.S.A.: implications for fault friction, state of stress and fluid pressure. Journal of Structural Geology 18, 927–944.
Oncken, O., von Winterfeld, C., Dittmar, U., 1999. Accretion of a rifted passive margin: the Late Paleozoic Rhenohercynian fold and thrust belt (Middle European Variscides). Tectonics 18, 75–91.
Passchier, C.W., Trouw, R.A.J., 1996. Microtectonics. Springer, Berlin.
Piecha, M., 2007. Vorläufiges Ergebnis der Conodontenuntersuchungen aus der Bohrung RWTH-1. Geological Survey NRW, Krefeld.
Ramsay, J.G., Huber, M., 1983. The Techniques of Modern Structural Geology. Vol. 1: Strain Analysis. Academic Press, London.
Ramsay, J.G., 1980. The crack-seal mechanism of rock deformation. Nature 284, 135–139.
Ribbert, K.H., 2006. Die Bohrung RWTH-1-Regionalstratigraphische Einordnung und Deutung. Geological Survey NRW, Krefeld.
Rottke, W., Stroink, L., 1999. Die Genese devonischer Vorlandsedimente am NW-Rand des Rheinischen Massivs – Zement- und Porenraumentwicklung. Zeitschrift der Deutschen Geologischen Gesellschaft 150, 471–491.
Salvini, F., Billi, A., Wise, D.U., 1999. Strike-slip fault-propagation cleavage in carbonate rocks: the Mattinata Fault Zone, Southern Apennines, Italy. Journal of Structural Geology 21, 1731–1749.
Schmidegg, O., 1928. Über geregeltes Wachstumsgefüge. Jahrbuch der Geologischen Bundesanstalt 78, 1–51.
Scholz, K., Urai, J.L., Trautwein, U., 2006. Microstructural analysis of the RWTH-1 cores in thinsections. In: 11. Symposium Tektonik, Struktur-und Kristallingeologie (TSK), Göttingen.
Sindern, S., Stanjek, H., Hilgers, C., Etoundi, Y., 2007. Short-term hydrothermal effects on the 'crystallinities' of illite and chlorite in the footwall of the Aachen-Faille du Midi thrust fault – first results of the RWTH-1 drilling project. Clays and Clay Minerals 55, 200–212.
Sindern, S., Warnsloh, J.M., Trautwein-Bruns, U., Chatziliadou, M., Becker, S., Yuceer, S., Hilgers, C., Kramm, U., 2008. Geochemical composition of sedimentary rocks and imprint of hydrothermal fluid flow at the Variscan front – an example from the RWTH-1 well (Germany). Zeitschrift der Deutschen Gesellschaft für Geowissenschaften 159, 623–640.
Soliva, R., Maerten, F., Petit, J.P., Auzias, V., 2010. Field evidences for the role of static friction on fracture orientation in extensional relays aling strike-slip faults; comparison with photoelasticity and 3D numerical modeling. Journal of Structural Geology 32, 1721–1731.
Taber, S., 1916. The origin of veins of the asbestiform minerals. Proceedings of the National Academy of Sciences 2, 659–664.
Thijssen, J.M., Knops, H.J.F., Dammers, A.J., 1992. Dynamic scaling in polycrystalline growth. Physical Review B 45, 8650–8656.
Trautwein-Bruns, U., Schulze, K.C., Becker, S., Kukla, P.A., Urai, J.L., 2010. In situ stress variations at the Variscan deformation front – results from the deep Aachen geothermal well. Tectonophysics 493, 196–211.
Tsukuda, T., 1985. Long-term seismic activity and present microseismicity on active faults in southwest Japan. Earthquake Prediction Research 3, 253–284.
Urai, J.L., Williams, P.F., van Roermund, H.L.M., 1991. Kinematics of crystal growth in syntectonic fibrous veins. Journal of Structural Geology 13, 823–836.
Walter, R., 2007. Geologie von Mitteleuropa. Schweizerbart'sche Verlagsbuchhandlung, Stuttgart.
Walter, R., 2010. Aachen und südliche Umgebung – Sammlung geologischer Führer, vol. 101. Gebr. Borntraeger, Berlin/Stuttgart.
Worum, G., Michon, L., van Balen, R.T., van Wees, J.D., Cloetingh, S., Pagnier, H., 2005. Pre-Neogene controls on present-day fault activity in the West Netherlands Basin and Roer Valley Rift System (southern Netherlands): role of variations in fault orientation in a uniform low-stress regime. Quaternary Science Reviews 24, 473–488.
Zijerveld, L., Stephenson, R., Cloetingh, S., Duin, E., Vandenberg, M.W., 1992. Subsidence analysis and modeling of the Roer Valley Graben (SE Netherlands). Tectonophysics 208, 159–171.